Beyond FFT: Precision Vibration Tracking with FMCW Radar and Kalman Estimators

Thomas Moon
Department of Electrical and Computer Engineering
University of Illinois at Urbana and Champaign
Urbana, USA.
tmoon@illinois.edu

***Abstract*—This paper introduces a novel approach to fast and precise vibration tracking using Frequency Modulated Continuous Wave (FMCW) radar augmented with Kalman estimators. The escalating demand for high-precision sensing across diverse applications underscores the need for radar systems capable of tracking dynamic targets with unprecedented accuracy. Traditional FFT-based FMCW radars often fall short in achieving the requisite speed and precision for real-time fine vibration tracking. Leveraging the inherent advantages of FMCW radar and Kalman estimators, an innovative solution is proposed to address this challenge. This paper details the state-space equations for FMCW radar, outlining the integration of FMCW radar with Kalman estimators and analyzing the lower and upper bounds of the trackability. Simulation results validate the efficacy of the approach, demonstrating significant advancements in tracking dynamic targets.**

***Index Terms*—FMCW radar, FFT, Kalman filter, Kalman smoother, Bayesian estimator, vibration tracking, radar signal processing**

I. Introduction

In recent years, the demand for high-precision sensing in various fields has surged, necessitating the development of advanced radar systems capable of tracking dynamic targets with unprecedented accuracy. Frequency Modulated Continuous Wave (FMCW) radar has emerged as a promising technology for such applications due to its ability to provide high-resolution range and velocity information.

Vibration tracking is a critical aspect of monitoring and controling systems in fields such as structural health monitoring [1], industrial automation [2], human vital signs [3], [4], robots [5], and autonomous vehicles [6]. Traditional radar systems often face challenges in achieving the required speed and accuracy for real-time vibration tracking. The integration of FMCW radar, characterized by its continuous wave transmission and frequency modulation, introduces a unique set of advantages, including improved range resolution and enhanced sensitivity to low-velocity movements.

Nevertheless, traditional methods for vibration tracking in FMCW radar [7]–[15] heavily depend on the Fast Fourier Transform (FFT), necessitating the accumulation of a batch of samples. This constraint imposes a limitation on the tracking speed, capping it at approximately 10 kHz. While this rate proves sufficient for monitoring human activities and vital signs, it falls short in capturing the rapid vibrations exhibited by mechanical devices like drones, robots, building structures, acoustic devices, or vehicles. The inherent swiftness of these mechanical dynamics exceeds the capability of conventional FFT-based approaches for accurate tracking. Similar approaches to the FFT, such as autoregressive methods or subspace-based methods (Capon, MUSIC, etc.) [16], also rely on a batch of samples, further limiting the tracking speed.

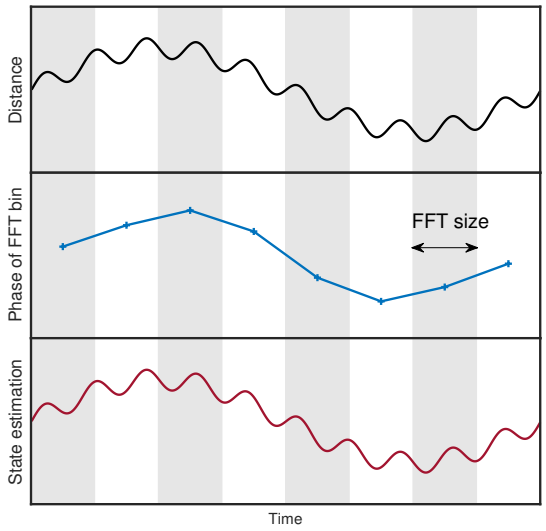

Fig. 1. Comparison of the actual distance of a vibrating target, the phase of the target FFT Bin, and the Kalman Estimator's state estimation.

To further elevate the performance of FMCW radar in vibration tracking scenarios, this paper proposes the utilization of a Kalman filter. The Kalman filter is a powerful estimation algorithm that optimally combines Gaussian-distributed noisy measurements with a dynamic system model, providing a robust and efficient means to estimate the true state of a target. By integrating the Kalman filter into the FMCW radar system, this work aims to mitigate the effects of measurement uncertainties and enhance the accuracy and responsiveness of vibration tracking.

While the combination of Kalman filter with FMCW radar is not novel, previous works [17]–[20] predominantly focused on leveraging Kalman filters to refine the accuracy of FFT-based phase tracking. Consequently, the tracking speed remained constrained by the FFT size. In contrast, this paper introduces

a novel approach by formulating a state-space model that describes the evolution of angle measurement and target vibration. Subsequently, the proposed work integrates the Kalman filter and smoother to estimate the state at every sample, thereby decoupling the tracking speed from the limitations imposed by the FFT size.

Figure 1 compares the vibration trackability between the conventional FFT-based FMCW radar and our innovative Kalman filter-based approach. Traditional methods rely on tracking the phase of the target FFT bin to estimate vibrations, limiting time-resolution due to the fixed FFT size. Additionally, accurately selecting the appropriate target bin poses a considerable challenge. In contrast, our proposed Kalman filter-based approach overcomes these limitations by enabling vibration estimation at higher time-resolution. This improvement stems from conducting estimations with each sample, rather than being constrained by the fixed intervals imposed by FFT processing.

This paper is structured as follows: Section II delves into the fundamental principles of FMCW radar and its challenges in fast dynamic target tracking. Section III presents the proposed methodology, constructing state-space equations for FMCW, detailing the integration of FMCW radar with a Kalman filter/smoother for fast and precise vibration tracking, and analyzing the upper/lower bounds of the trackability of the proposed estimator. Section IV discusses the simulated experimental setup and presents results validating the efficacy of the proposed approach. Finally, Section V concludes the paper, summarizing key findings and outlining directions for future research in the realm of high-precision sensing using FMCW radar.

II. FMCW Primary for Vibration

FMCW radar operates by continuously emitting periodic pulses with a linearly sweeping frequency over time, illustrated by the blue line in Figure 2 (a). Mathematically, the transmitted signal is defined as

$$s_t(t) = \exp\left(j2\pi\left(f_c t + \frac{S}{2}t^2\right)\right), \tag{1}$$

where f_c and S represent the starting frequency and slope of the FMCW chirp, respectively. The reflected signal, depicted by the red line in Figure 2 (a), is a time-delayed version of the transmitted signal, resulting from its interaction with a target. The time-of-flight (TOF, τ) is the elapsed time for the transmitted signal to travel the round-trip distance $2d$ from the radar to the target and back. Assuming a single target in the scene, the received signal is expressed as $s_r(t) = As_t(t-\tau)$, with A denoting the attenuation factor of the target. The receiver mixes the transmitted and received signals, producing a beat signal $x(t) = s_r(t) \cdot s_t(t)^*$, as depicted in Figure 2 (b).

For a stationary target, the beat signal simplifies to

$$x(t) = A\exp\left(j2\pi\left(S\tau t + f_c\tau - \frac{S}{2}\tau^2\right)\right) \tag{2}$$

$$\approx A\exp\left(j2\pi\left(S\tau t + f_c\tau\right)\right). \tag{3}$$

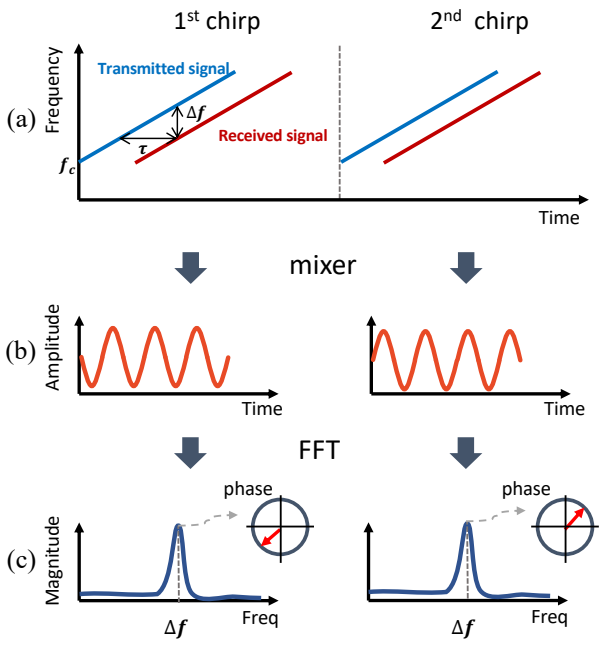

Fig. 2. (a) The figure shows the transmitted FMCW signal (blue) and its reflected signal (red). The time-of-flight (τ) between the two signals maps to the frequency shift Δf. (b) Mixing the transmitted and reflected signals yields the beat signal whose frequency is Δf. (c) The FFT peak corresponds to Δf. A subtle change in the distance over the chirps shifts the phase of the FFT peak.

This characteristic allows the extraction of a distance profile for the targets, as the frequency of the beat signal (Δf) is $S\tau$, where S is a known parameter. Consequently, performing the FFT on the beat signal enables the estimation of Δf, facilitating the measurement of the target distance through $d = c\frac{\tau}{2} = c\frac{\Delta f}{2S}$, where c represents the speed of light, approximately 3×10^8m/s.

A. Challenges for Fast-Vibrating Target

When the target moves or vibrates over time, τ is no longer constant. The beat signal for the vibrating target is

$$x(t) = A\exp\Big(j2\pi(S\tau(t)t + f_c\tau(t))\Big), \tag{4}$$

where $\tau(t)$ is the TOF of the target in d_0 with the small displacement $d(t)$. The time-varying TOF can be expressed as

$$\tau(t) = \frac{2d_0}{c} + \frac{2d(t)}{c}. \tag{5}$$

In scenarios where the frequency change is smaller than the FFT bin resolution, Figure 2 (c) illustrates that the peaks of the FFT magnitudes during the first and second chirp remain unchanged. Nevertheless, despite the stability of these peaks, the phase of the FFT is still detectable.

Previous studies [7]–[15] have harnessed this phase change to monitor slight variations in target distance. However, these approaches exhibit limitations; the time resolution of tracking is inherently bound by the FFT size. Consequently, rapid distance changes occurring within the FFT duration are averaged

out to a single phase value. Additionally, accurately selecting the appropriate FFT bin is critical for precise tracking [8], [11], [13]. When distance changes span multiple FFT bins, spectral leakage degrades phase estimation performance. Another challenge is the difficulty in identifying the correct target bin due to the non-obvious shape of the spectrum. Since $\tau(t)$ is time-varying, the beat signal in (4) experiences frequency modulation (FM) and phase modulation (PM). In cases of small vibrations, the beat signal is modeled as a narrow-band signal dominated by a single tone in its spectrum, facilitating vibration estimation through phase tracking. However, fast vibrations necessitate modeling as a wide-band FM/PM modulation signal, resulting in a spectrum that is no longer composed of a single tone.

To address this issue, this paper introduces a Bayesian estimation technique for tracking the time-varying $\tau(t)$. While the prevalent FFT-based techniques in FMCW signal processing can only track $\tau(t)$ in chirp-wise time resolution, the proposed technique enables sample-wise time resolution for enhanced precision in tracking.

III. Proposed Fast Vibration Estimator

A. State-space Equations for FMCW

Let the angle of (4) be $\theta(t)$. One can express $\theta(t)$ and its first derivative $\frac{d\theta}{dt}$ as the following.

$$\theta(t) = 2\pi S\tau(t)t + 2\pi f_c\tau(t), \tag{6}$$

$$\frac{d\theta}{dt} = 2\pi S\tau(t) + 2\pi S\tau'(t)t + 2\pi f_c\tau'(t), \tag{7}$$

where $\tau'(t) = \frac{d\tau(t)}{dt}$. Because the function $\tau(t)$ is unknown but perturbing, we use the Wiener velocity model, where the derivative of the velocity ($\tau'(t)$) is a random process, $\mathbf{w}(t)$ [21].

Consequently, we can construct a *time-variant* continuous-time linear model expressed as a stochastic differential equation (SDE),

$$\frac{d\mathbf{m}(t)}{dt} = \mathbf{F}(t)\mathbf{m}(t) + \mathbf{L}\mathbf{w}(t), \tag{8}$$

where $\mathbf{m}(t) = \begin{bmatrix}\theta(t)\\ \tau(t)\\ \tau'(t)\end{bmatrix}$, $\mathbf{F}(t) = \begin{bmatrix}0 & 2\pi S & 2\pi(f_c + St)\\ 0 & 0 & 1\\ 0 & 0 & 0\end{bmatrix}$, and $\mathbf{L} = \begin{bmatrix}0\\ 0\\ 1\end{bmatrix}$.

This work aims to estimate $\tau(t)$ every discrete sample rather than every chirp using the FFT. In order to estimate the state in discrete time, the continuous-time model in (8) is discretized by the state transition matrix computed by the fundamental matrix of (8) [22].

As a result, the discrete dynamic model is given by

$$\mathbf{m_k} = \mathbf{A_{k-1}}\mathbf{m_{k-1}} + \mathbf{q_{k-1}}, \tag{9}$$

where $\mathbf{q_{k-1}}$ is a zero-mean discrete-time Gaussian noise process with covariance matrix $\mathbf{Q}$. The discrete state at time t_k is

$$\mathbf{m_k} = \begin{bmatrix}\theta(t_k)\\ \tau(t_k)\\ \tau'(t_k)\end{bmatrix}, \tag{10}$$

and the transition matrix is given as

$$\mathbf{A_{k-1}} = \begin{bmatrix}1 & 2\pi S\Delta t & 2\pi f_c\Delta t + 2\pi S\Delta t\, t_{k-1}\\ 0 & 1 & \Delta t\\ 0 & 0 & 1\end{bmatrix}, \tag{11}$$

where $\Delta t = t_k - t_{k-1}$. It is worth noting that $\mathbf{A_{k-1}}$ includes *a time-dependent term* t_{k-1} due to the time-variant system in (8).

Let the noisy angle measurement of the beat signal be y_k sampled at the kth time index with the sampling period T_s, i.e., $\angle x(kT_s) = \angle\mathbf{x_k} = \mathbf{y_k}$ for $1 \le k \le N$. This means the measurement $\mathbf{y_k}$ is calculated by $\tan^{-1}(\mathbf{x_k})$ whose output is wrapped around $[-\pi, \pi]$. However, the angle θ in (6) can evolve beyond $[-\pi, \pi]$ as time increases. Hence, unwrapping the measured angle $\mathbf{y_k}$ is needed before the state estimation. Algorithm 1 explains the unwrapping process.

Algorithm 1 Angle Measurement Unwrapping

```
y_{1:N} = tan^{-1}(x_{1:N})
for k = 2 : N do
    if y_k − y_{k−1} > π then
        y_k = y_{k−1} − 2π
    else if y_k − y_{k−1} < −π then
        y_k = y_{k−1} + 2π
    else
        y_k = y_k
    end if
end for
```

Connecting the unwrapped $\mathbf{y_k}$ with the state vector $\mathbf{m_k}$, the measurement system can be described as

$$\mathbf{y_k} = \mathbf{H}\mathbf{m_k} + r_k, \tag{12}$$

where $\mathbf{H} = [1 \quad 0 \quad 0]$ and r_k a zero-mean discrete-time Gaussian noise process with variance σ^2.

B. Kalman Estimators with Unwrapping Angle

Based on the discrete state system in (9) and (12), the Kalman filter equations [21] can iteratively yield the estimate of $\mathbf{m_k}$ in two steps a) prediction and b) update. In the prediction step, the state $\mathbf{m_k^-}$ and the error covariance matrix $\mathbf{P_k^-}$ are computed from the previous ones in time step, $k-1$, as

$$\mathbf{m_k^-} = \mathbf{A_{k-1}}\mathbf{m_{k-1}}, \tag{13}$$

$$\mathbf{P_k^-} = \mathbf{A_{k-1}}\mathbf{P_{k-1}}\mathbf{A_{k-1}^T} + \mathbf{Q}. \tag{14}$$

Once the prediction is made, the state is updated with the measurement $\mathbf{y_k}$ as follows.

$$\mathbf{S_k} = \mathbf{H}\mathbf{P_k^-}\mathbf{H^T} + \sigma^2, \tag{15}$$

$$\mathbf{K_k} = \mathbf{P_k^-}\mathbf{H^T}\mathbf{S_k^{-1}}, \tag{16}$$

$$\mathbf{m_k} = \mathbf{m_k^-} + \mathbf{K_k}[\mathbf{y_k} - \mathbf{H}\mathbf{m_k^-}], \tag{17}$$

$$\mathbf{P_k} = \mathbf{P_k^-} - \mathbf{K_k}\mathbf{S_k}\mathbf{K_k^T}. \tag{18}$$

Note that $\mathbf{S_k} = \mathbf{H}\mathbf{P_k^-}\mathbf{H^T} + \sigma^2$ is scalar because the measurement is scalar in (12). The innovation, which is the difference between the angle measurement $\mathbf{y_k}$ and the predicted measurement $\mathbf{H}\mathbf{m_k^-}$, is multiplied by the optimal Kalman gain $\mathbf{K_k}$ to refine the current state as shown in (17). In the next section, we will discuss the contribution of the 2π wrapping angle measurement to the state estimation.

In the practical FMCW radar systems, each set of N samples, representing measurements during a chirp, is stored in a buffer and subsequently streamed to the output. This characteristic allows the application of a Kalman smoother to reconstruct states preceding the current time. In contrast, the Kalman filter exclusively computes the present state of the system based on the previous measurements. The backward recursion equations for the fixed interval Kalman smoother are given as

$$\mathbf{m_{k+1}^-} = \mathbf{A_k}\mathbf{m_k}, \tag{19}$$

$$\mathbf{P_{k+1}^-} = \mathbf{A_k}\mathbf{P_k}\mathbf{A_k^T} + \mathbf{Q}, \tag{20}$$

$$\mathbf{G_k} = \mathbf{P_k}\mathbf{A_k^T}\mathbf{P_{k+1}^{-1}}, \tag{21}$$

$$\mathbf{m_k^s} = \mathbf{m_k} + \mathbf{G_k}[\mathbf{m_{k+1}^s} - \mathbf{m_{k+1}^-}], \tag{22}$$

$$\mathbf{P_k^s} = \mathbf{P_k} + \mathbf{G_k}[\mathbf{P_{k+1}^s} - \mathbf{P_{k+1}^{-1}}]\mathbf{G_k^T}, \tag{23}$$

where $\mathbf{m_k}$ and $\mathbf{P_k}$ are the estimated state and the error covariance matrix computed by the Kalman filter equations in (17) and (18).

C. Tracking Limits

The 2π wrapping angle in the measurement system in (12) limits the maximum trackable dynamics in the state. In order to avoid phase ambiguity, the two consecutive angles should be within $\pm\pi$. Let the two consecutive angles be θ_k and θ_{k-1}. By (9), the angle evolution can be expressed as

$$\theta_k = \theta_{k-1} + 2\pi S\Delta t\,\tau_{k-1} + 2\pi(f_c + St_{k-1})\Delta t\,\tau'_{k-1}.$$

In order to avoid the 2π ambiguity by the angular evolution terms, the following condition should be met:

$$\left|2\pi S\Delta t\,\tau_{k-1} + 2\pi(f_c + St_{k-1})\Delta t\,\tau'_{k-1}\right| < \pi.$$

Simplifying the condition by dividing by π and approximating $f_c + St_{k-1}$ with the average frequency of the chirp signal, f_0, the inequality becomes

$$\left|2S\Delta t\,\tau_{k-1} + 2f_0\Delta t\,\tau'_{k-1}\right| < 1.$$

Converting τ and τ' to the distance (d) and velocity (v) of the target, the condition is updated by

$$\left|\frac{4S\Delta t}{c}d_{k-1} + \frac{4f_0\Delta t}{c}v_{k-1}\right| < 1.$$

Assume the target is vibrating at the average nominal distance, $d_0 \approx d_{k-1}$, the upper and lower bounds can be computed in terms of the velocity of the vibration as

$$\frac{-1-M}{L} < v < \frac{1-M}{L}, \tag{24}$$

where $L = \frac{4f_0\Delta t}{c}$ and $M = \frac{4S\Delta t d_0}{c}$.

For a more tangible understanding of the bounds within a practical radar setup, envision an FMCW radar operating at a frequency of 77GHz (f_0), with a slope rate of 30MHz/μs (S), and an ADC sampling rate of 3MHz ($1/\Delta t$). Assume this radar senses a target located 1m away (d_0). According to (24), the proposed estimator theoretically spans a range of radial velocities from -3,312 m/s (towards the radar) to 2,533 m/s (away from the radar). The asymmetry in these bounds stems from the 1m distance to the target, introducing a positive frequency in the signal and consequently creating a smaller margin for positive velocities.

IV. Simulation

To assess the efficacy of the proposed estimator, simulations are conducted using an FMCW radar system with a vibrating target, exploring three distinct scenarios featuring varying vibration characteristics. In Scenario I, the vibration is modeled using the Wiener velocity model [21], where the velocity derivative follows a white Gaussian random process $\mathbf{w}(t)$. Scenario II introduces a modified Wiener velocity model, incorporating a sinusoidal oscillation into the velocity derivative. Scenario III investigates the estimator's behavior when confronted with vibrations exceeding the established tracking limits. The simulation employed FMCW radar parameters detailed in Table I, chosen to align with a commercial FMCW radar setup, specifically the Texas Instrument TI-IWR1843.

For clarity and ease of interpretation, the results are presented in distance and velocity units derived from τ and τ' by employing a simple scaling transformation, i.e., $d = \frac{c\tau}{2}$.

It is crucial to note that the time range depicted in the resulting figures corresponds to a single chirp period. Unlike conventional FFT-based approaches limited to reporting a single estimation, our proposed method excels in tracking fine changes occurring within the chirp period. This distinction underscores the superior temporal resolution of our approach compared to traditional methods.

A. Scenario I

In Scenario I, the vibration is characterized by the Wiener velocity model, with the derivative of the velocity denoted as $\mathbf{w_{sc1}}(t)$, following a Gaussian distribution with zero mean. The resulting simulated vibration exhibits a 9 cm pitch and a peak velocity of -2,685 m/s during the chirp period. In this specific radar configuration, the proposed estimator theoretically spans a detection range from -3,312 m/s to 2,533 m/s, as defined by (24). As illustrated in Figure 3, both distance and velocity are effectively tracked since the maximum velocity falls within the established bounds.

TABLE I
SIMULATION SETUP

	Parameter	Value
FMCW	f_c	77 GHz
	Sampling rate	3 MHz
	# of total samples	256
	Slope	30 MHz/μs
	Chirp period	85 μs
Target	Distance (m)	1
	Vibration Type	See Scenario I, II, III

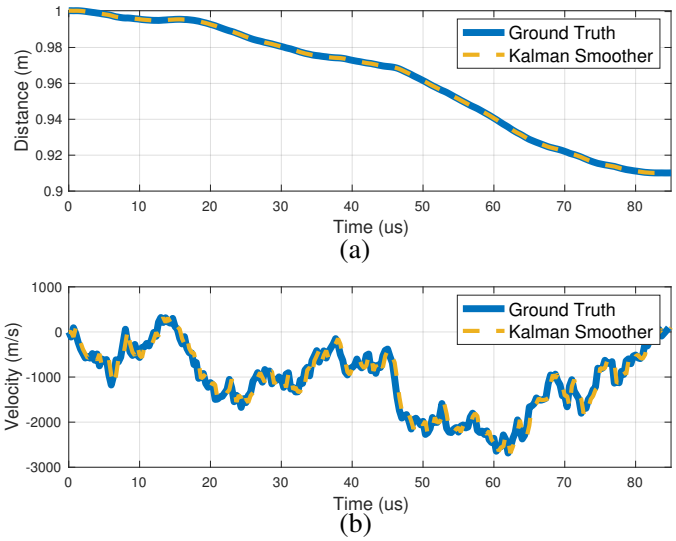

Fig. 3. Ground truth and estimated distance and velocity of the simulated vibration in Scenario I.

B. Scenario II

In Scenario II, a modified Wiener velocity model is employed to characterize the vibration. The derivative of the velocity is a random process featuring a sinusoidal oscillation, expressed as $\mathbf{w_{sc2}}(t) = \mathbf{w_{sc1}}(t) + A\sin(2\pi f_m t)$. We set $f_m = 20kHz$, resulting in approximately 1.7 periods within the chirp period. The simulated vibration in this scenario produces a 2 cm pitch and a peak velocity of -1,118 m/s. As evident in Figure 4, both distance and velocity are effectively tracked, given that the maximum velocity falls within the established bounds.

C. Scenario III

Scenario III investigates the performance of the estimator when confronted with vibrations surpassing the predefined tracking limits. The simulated vibration, resembling the conditions in Scenario II but featuring more extensive movement, generates a pitch of 26 cm and a maximum velocity of 7,550 m/s—exceeding the established tracking bounds. Figures 5 (a) and (b) visually depict the failure of distance and velocity tracking under these circumstances. This failure arises from

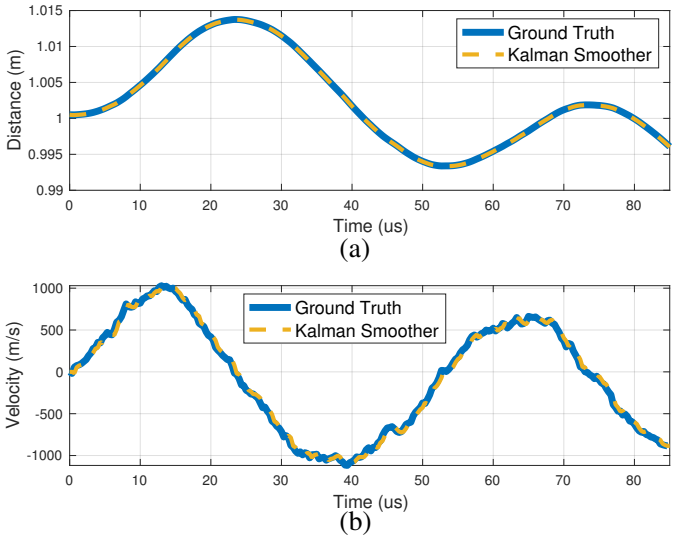

Fig. 4. Ground truth and estimated distance and velocity of the simulated vibration in Scenario II.

the considerable movement inducing a 2π ambiguity in angle measurements. As detailed in Section III-C, our proposed estimator demonstrates effective tracking only when the angle rotation remains below $\pm\pi$ in the subsequent sample. The innovation plot in Figure 5 (c) illustrates deviations in radians ($\mathbf{y_k} - \mathbf{H}\bar{\mathbf{m}}_\mathbf{k}$) within the Kalman filter equations (13). Notably, the state estimation encounters challenges whenever the innovations extend beyond $\pm 2\pi$, a consequence of the pronounced movement.

D. Monte Carlo Experiments

For each scenario, the Kalman estimator is simulated by 100 Monte Carlo (MC) runs. Figure 6 illustrates the empirical cumulative density function (CDF) of Root Mean Square (RMS) errors for distance and velocity, presented in a logarithmic scale (dB). Specifically, Figure 6 (a) and (b) depict the CDFs for distance and velocity across the three scenarios, respectively. In scenarios where the targets remain within the tracking limits (Scenario I and Scenario II), the RMS error is negligible. However, when vibrations exceed these limits (Scenario III), the estimation errors for both distance and velocity become significant.

V. CONCLUSION

This paper addresses the imperative need for high-precision sensing in various applications by leveraging the capabilities of FMCW radar. Recognizing the challenges inherent in traditional radar systems, particularly in achieving real-time and high-accuracy vibration tracking, our proposed Kalman filter-based approach represents a significant advancement. By introducing a state-space model that characterizes the evolution of angle measurement and target vibration, this paper successfully decouples the tracking speed from the constraints imposed by the FFT size. The integration of the Kalman filter

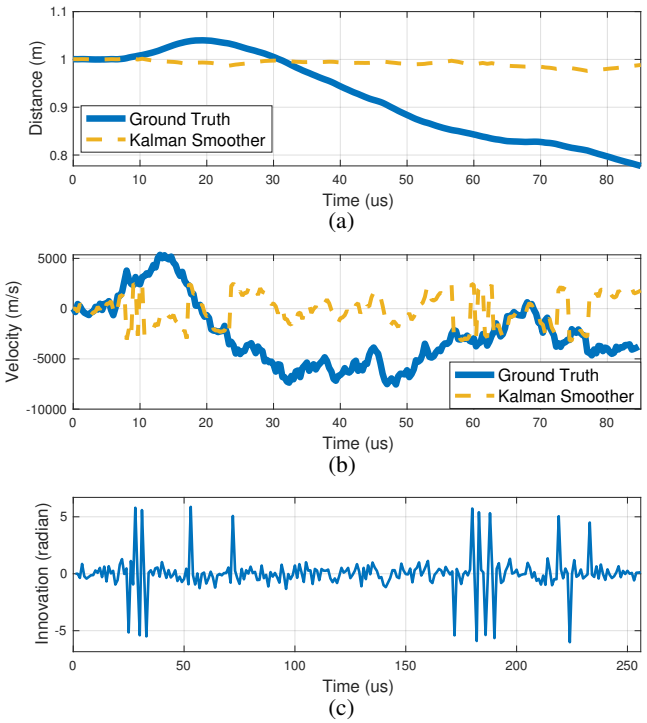

Fig. 5. (a) (b) Ground truth and estimated distance and velocity of the simulated vibration in Scenario III. (c) Innovation of the Kalman filter in radian.

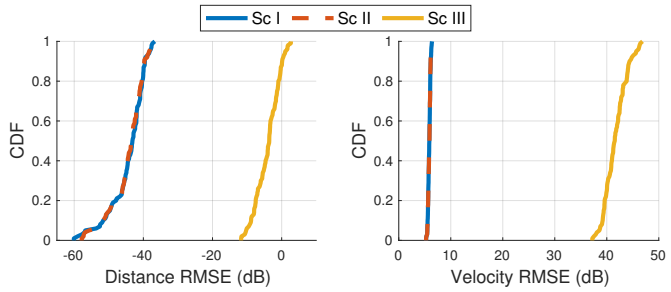

Fig. 6. Cumulative RMSE probability function for distance and velocity across Scenario I, II, and III.

at every sample enhances time-resolution, surpassing the limitations of traditional FFT-based approaches. Our simulation results validate the efficacy of the proposed approach, demonstrating its ability to accurately and swiftly track fast dynamic targets. This achievement is crucial for applications ranging from structural health monitoring to industrial automation and autonomous vehicles.

In conclusion, this paper not only contributes a novel methodology for enhancing FMCW radar's performance in vibration tracking but also opens avenues for further research in high-precision sensing. As technology continues to evolve, the proposed Kalman filter-based approach lays the foundation for advancing radar systems to meet the increasing demands of precision sensing in diverse fields.

For future research, we aim to extend our efforts by incorporating comprehensive parameter estimation, encompassing state and measurement noise variance, exploring scenarios involving non-Gaussian noise and multiple target tracking, and addressing practical challenges including model mismatches in hardware measurements.

REFERENCES

[1] D. Montalvao, N. M. M. Maia, and A. M. R. Ribeiro, "A review of vibration-based structural health monitoring with special emphasis on composite materials," *Shock and vibration digest*, vol. 38, no. 4, pp. 295–324, 2006.

[2] R. B. Randall, *Vibration-based condition monitoring: industrial, automotive and aerospace applications*. John Wiley & Sons, 2021.

[3] M. Kebe, R. Gadhafi, B. Mohammad, M. Sanduleanu, H. Saleh, and M. Al-Qutayri, "Human vital signs detection methods and potential using radars: A review," *Sensors*, vol. 20, no. 5, p. 1454, 2020.

[4] D. Dias and J. Paulo Silva Cunha, "Wearable health devices—vital sign monitoring, systems and technologies," *Sensors*, vol. 18, no. 8, p. 2414, 2018.

[5] H. E. Taha, M. Kiani, T. L. Hedrick, and J. S. Greeter, "Vibrational control: A hidden stabilization mechanism in insect flight," *Science robotics*, vol. 5, no. 46, p. eabb1502, 2020.

[6] M. S. Qatu, M. K. Abdelhamid, J. Pang, and G. Sheng, "Overview of automotive noise and vibration," *International Journal of Vehicle Noise and Vibration*, vol. 5, no. 1-2, pp. 1–35, 2009.

[7] J. Kim, S. Lim, J. Jung, and S.-C. Kim, "Two-stage clutter suppression method for human detection using fmcw radar," in *2023 IEEE Radar Conference (RadarConf23)*. IEEE, 2023, pp. 1–6.

[8] M. Shin, Y. Jung, J. Kim, K. Choi, K. Lee, H. Ju, K.-I. Cho, and S. Lee, "Fmcw radar-based vital signal monitoring technique using adaptive range-bin selection," in *2023 IEEE Radar Conference (RadarConf23)*. IEEE, 2023, pp. 1–6.

[9] I. Lenz, Y. Rong, and D. W. Bliss, "Radarcardiograph signal modeling and time-frequency analysis," in *2023 IEEE Radar Conference (RadarConf23)*. IEEE, 2023, pp. 1–6.

[10] H. Lee, B.-H. Kim, J.-K. Park, and J.-G. Yook, "A novel vital-sign sensing algorithm for multiple subjects based on 24-ghz fmcw doppler radar," *Remote Sensing*, vol. 11, no. 10, p. 1237, 2019.

[11] H.-I. Choi, H. Song, and H.-C. Shin, "Target range selection of fmcw radar for accurate vital information extraction," *IEEE Access*, vol. 9, pp. 1261–1270, 2020.

[12] M. Alizadeh, G. Shaker, J. C. M. De Almeida, P. P. Morita, and S. Safavi-Naeini, "Remote monitoring of human vital signs using mm-wave fmcw radar," *IEEE Access*, vol. 7, pp. 54 958–54 968, 2019.

[13] B. Zhang, B. Jiang, R. Zheng, X. Zhang, J. Li, and Q. Xu, "Pi-vimo: Physiology-inspired robust vital sign monitoring using mmwave radars," *ACM Transactions on Internet of Things*, vol. 4, no. 2, pp. 1–27, 2023.

[14] L. Piotrowsky and N. Pohl, "Spatially resolved fast-time vibrometry using ultrawideband fmcw radar systems," *IEEE Transactions on Microwave Theory and Techniques*, vol. 69, no. 1, pp. 1082–1095, 2020.

[15] Y. Xiong, Z. Peng, G. Xing, W. Zhang, and G. Meng, "Accurate and robust displacement measurement for fmcw radar vibration monitoring," *IEEE Sensors Journal*, vol. 18, no. 3, pp. 1131–1139, 2017.

[16] M. H. Hayes, *Statistical digital signal processing and modeling*. John Wiley & Sons, 1996.

[17] M. Lipka, E. Sippel, and M. Vossiek, "An extended kalman filter for direct, real-time, phase-based high precision indoor localization," *IEEE Access*, vol. 7, pp. 25 288–25 297, 2019.

[18] G. Su, N. Petrov, and A. Yarovoy, "Dynamic estimation of vital signs with mm-wave fmcw radar," in *2020 17th European Radar Conference (EuRAD)*. IEEE, 2021, pp. 206–209.

[19] P. Vaishnav and A. Santra, "Continuous human activity classification with unscented kalman filter tracking using fmcw radar," *IEEE Sensors Letters*, vol. 4, no. 5, pp. 1–4, 2020.

[20] M. Arsalan, A. Santra, and C. Will, "Improved contactless heartbeat estimation in fmcw radar via kalman filter tracking," *IEEE Sensors Letters*, vol. 4, no. 5, pp. 1–4, 2020.

[21] S. Särkkä and L. Svensson, *Bayesian filtering and smoothing*. Cambridge university press, 2023, vol. 17.

[22] C.-T. Chen, "Linear system theory and design," 1999.